

Contents list available at **IJND**
International Journal of Nano Dimension

Journal homepage: www.IJND.ir

Structure of Lattice Strain and effect of sol concentration on the characterization of $\text{TiO}_2\text{-CuO-SiO}_2$ nanoparticles

ABSTRACT

M. Riazian¹

A. Bahari^{2*}

¹Department of Engineering,
Tonekabon Branch, Islamic Azad
University, Tonekabon, Iran.

²Department of physics,
university of Mazandaran,
Babolsar, Iran.

Received: 14 January 2012

Accepted: 16 April 2012

We report on the synthesis, morphology, chemically and structurally of $\text{TiO}_2\text{-CuO-SiO}_2$ nanostructure with different precursors molar ratio and calcined temperatures. In the present work, ternary reactive powders in the $\text{TiO}_2\text{-CuO-SiO}_2$ systems have been obtained using the sol-gel method, by the simultaneous gelation of all cations. The compounds and other elements change in special chemical and physical qualities in this nano oxide. Powders and coatings have been characterized by XRD, SEM, EDX and FTIR. X-ray diffraction showed the formation of nano crystalline CuO (Tenorite) and anatase phases. The average crystallite size was calculated by using X-ray diffraction analysis. The activation energy (E) of nanoparticles formation during thermal treatment were calculated. The lattice strain evaluated by Williamson-Hall's equation. SEM revealed that nanoaggregation structure formed by increasing the calcined temperature and grains like to make a spherical shape. EDX spectroscopy confirmed the composition of the ternary powders and coating, which are formed during the gelation process. FTIR spectra showed that Si-O-Ti, Ti-O, Cu-O, Ti-O-Ti, Ti-OH and Si-O-Si bonds are formed and indicated that titanium is in four-fold coordination with oxygen in the SiO_4^{4-} . The effects of chemical compositions and the strong process on the surface topography and the crystallization of anatase and CuO (Tenorite) were studied. With increasing the molar ratio (content of CuO) in as-prepared state, the formation of rod region was more prominent than agglomerate region.

Keywords: Nanostructure; Poly-component; $\text{TiO}_2\text{-CuO-SiO}_2$; Activation Energy and Sol-Gel method.

* Corresponding author:

A. Bahari

Department of physics, university
of Mazandaran, Babolsar, Iran.

Tel +98 9112537702

Fax +98 1125342480

Email a.bahari@umz.ac.ir

INTRODUCTION

Titania is known to have three natural polymorphs, i.e. rutile, anatase, and brookite. Only anatase is generally accepted to have a significant photocatalytic activity.

The photocatalytic performance of these compounds depends on the characteristic of the TiO_2 crystallites, such as the size and surface area. Therefore, modification of its physical and chemical property is of interest to researchers. One of the possible ways to modify the property of TiO_2 crystallites is by adding a second semiconductor into the TiO_2 matrix. SiO_2 has high thermal stability, excellent mechanical strength and help to create new catalytic sites due to the interaction between TiO_2 and SiO_2 [1] also, SiO_2 acts as a carrier of TiO_2 and helps to obtain a large surface area as well as a suitable porous structure [2]. During the last years many studies dealing with TiO_2 doping with different metals have shown the alterations that the dopant may cause the structural properties. For instance, it has been indicated that the insertion of Cu nanoparticles in the TiO_2 rutile lattice improves its photocatalytic efficiency [3].

Titania can be synthesized by various techniques, such as precipitation [4], chemical vapor deposition [5], hydrothermal method [6] and glycothermal method [7]. Another common technique that can result in Titania with extremely high surface area is sol-gel method. The sol-gel process is one of the versatile methods to prepare ceramic materials. The incorporation of an active metal in the sol during the gelation stage allows the metal to have a direct interaction with support. The sol-gel process is commonly applied to the synthesis such as TiO_2 materials because of its several advantages such as low temperature processing and the ability to prepare materials in various shapes, compared with the conventional preparation procedures of glass and ceramics. [8,9].

It is well recognized that the properties of materials highly depend on size, morphology, and dimensionality [10], three crucial geometric parameters. Many chemical and physical routes are explored by the chemists and material researchers to control those parameters and to obtain various shapes of materials such as tubes, rods, plates, and so on [11].

Among all metal oxides, TiO_2 powders are extensively used as catalysts, adsorbents, composites, ceramics, and catalyst supports because of their high surface area and significant pore volume. In this work, we prepare TiO_2 -CuO- SiO_2 by using hydrolysis procedure of Tetra isopropyl ortho titanate and copper nitrate which is transformed to anatase and CuO by heating it at 300, 500 and 800°C. It obviously depends on the preparation procedures and TiO_2 content in combination.

EXPERIMENTAL

The composition of the starting solution and the experimental conditions used for ternary powders are listed in Table 1. Figure 1 illustrates the preparation procedures. The precursors: tetraethoxysilane (TEOS, Merk, $\geq 99\%$), tetra isopropyl ortho titanate (TIOT, Merk $\geq 98\%$), $\text{Cu}(\text{NO}_3)_2 \cdot 3\text{H}_2\text{O}$ (aplichem), acetic acid (Floka, 60.5%), HCl (Merk, 36%), Ethanol (Merk $\geq 97\%$) and deionized water were used without further purification.

Table 1. Composition of starting solutions and experimental conditions for ternary powders preparation.

Sol-gel Method used	Sol-gel Method step	Precursor	Molar ratio(MR) TEOS/ TIOT / Copper nitrite =1:1/0.5 TEOS/Copper nitrite/TIOT=1:1/1	Stirring Time(h)	PH
Alkoxide route	1	TEOS TIOT	TEOS/EtOH/HCl/H ₂ O =1:50/0.1/2 TIOT/EtOH/CH ₃ COOH/H ₂ O =1:50/4/2	0.5	3
	2	$\text{Cu}(\text{NO}_3)_2 \cdot 3\text{H}_2\text{O}$	$\text{Cu}(\text{NO}_3)_2 \cdot 3\text{H}_2\text{O}/\text{H}_2\text{O} = 1:0.02$	0.5	2

Acetic acid acts an important role in hydrolysis because chelating mechanism decreases the rate of hydrolysis, meaning very fine particles of titanium hydroxide will be formed and suspended in solution. In MR=0.5, the molar ratio of TEOS and TIOT in combination is twice of molar ratio of copper nitrate and in MR=1, the molar ratio of TEOS, TIOT and copper nitrate in precursors combination are equal. After 48 hours gelation was formed. Afterward, the gel was dried for about 24 hours at 50 °C temperature in air and calcined in three different temperatures (300, 600 and 800 °C). Moreover, the effects of varied calcinations temperature were studied as a prepared, 300, 600 and 800 °C.

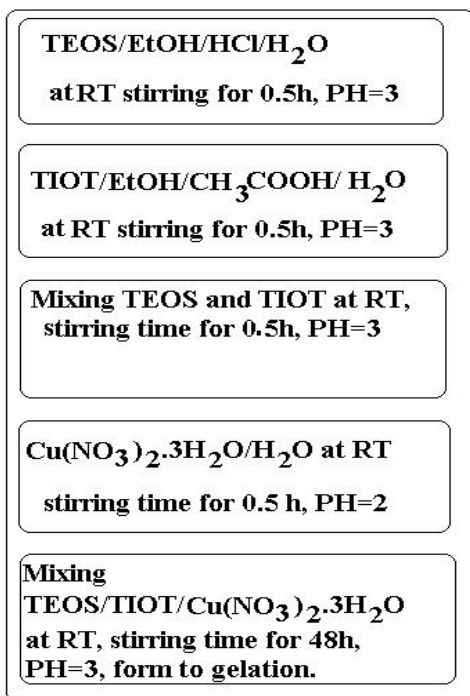


Fig. 1. Schematic flow chart illustrating the steps in the synthesis pathway of $\text{TiO}_2\text{-CuO-SiO}_2$ nanomaterials.

Characterization of the $\text{TiO}_2\text{-CuO-SiO}_2$

• X-ray powder diffraction study

X-ray powder diffraction (XRD) patterns were measured on a (GBC-MMA 007 (2000)) X-ray diffractometer. The diffractograms were recorded with ($K_\alpha(\text{Cu})$, 1.54 \AA , 0.02° step size in which the speed was $10 \frac{\text{deg}}{\text{min}}$) radiation over a 2θ range of $10^\circ - 80^\circ$.

• Scanning electron microscopy

SEM (XL30 Philips) was routinely used to investigate the morphology of the nano-particles.

• FT-IR study

FT-IR measurements were performed on a 1730 Infrared Fourier Transform Spectrometer (Perkin-Elmer) using the potassium bromide as the background.

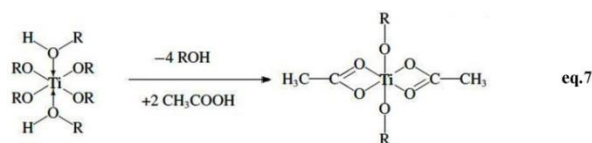
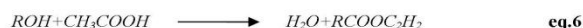
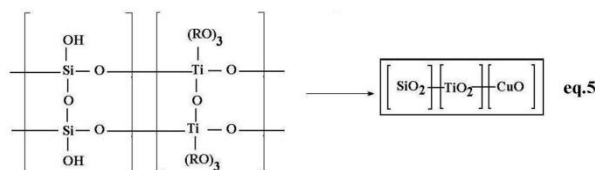
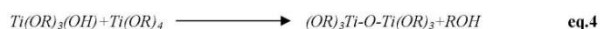
RESULTS AND DISCUSSION

In the sol-gel method, two factors determine the hydrolysis and condensation rates. The first factor is the acetic acid, which promotes the hydrolysis of TEOS; the second is the titanate formed by the chelate of acetic acid and titanium, which accelerates the condensation of TEOS [12]. With respect to acetic acid, it plays two roles in the system. From one side, it acts as the catalyst to promote the hydrolysis of TEOS; on the other side, it chelates with titanium to form titanate, which accelerate the condensation of TEOS and retard the hydrolysis and condensation of TIOT. In the present work, the TEOS is partially hydrolyzed in ethanol, water and hydrochloric acid under controlled conditions that allow the solution, i.e., sol, to yield a formable, loosely cross-linked matrix, i.e., gel. Then, titanium chelate compound (PTP) was added to form polytitanosiloxane solution (TiSi) via polycondensation reaction (eqs. 1 and 5). $\text{TiO}_2\text{-CuO-SiO}_2$ precursor solution consists of siloxane (Si-O-Si) and Si-O-Ti linkages as a main chain.

Titanium alkoxide is hydrolyzed and condensed to form polymeric species composed of M-O-M bonds in ethanol solution. The process is generally described in (eqs. 2-4).

Hydrolyzing water can be supplied via two different mechanisms. The first mechanism is the esterification of Ethanol and acetic in situ, as shown in (eq. 4). The second one is the oxolation, as shown in (eq.3). The esterification product, butyl acetate was found and identified by a GC/Mass (HP GCD plus). The esterification becomes much more favorable when the ratio of acetic acid/metal alkoxide is low [13]. Acetic acid also serves as a chelating ligand and can change the alkoxide precursor at the molecular level, thus modifying the hydrolysis process [14]. Chelation can be described

in (eqs. 6 and 7) [15]. The hydrolysis of chelated titanium complex is deferred so that Ethanol ligand may still remain in the sol. Upon further hydrolysis, Ethanol ligand is broken off and gives to Ti–OH bond. This mechanism decreases the rate of hydrolysis, meaning very fine particles of titanium hydroxide will be formed and suspended in solution.



Crystallographic phases of the composite ceramic membranes were investigated by XRD method. Figures 2 and 3 and assignments of the XRD peaks are summarized in Tables 1 and 2, respectively. Due to different hydrothermal treatment crystalline phases are formed. Figures 2 and 3 show the XRD patterns of powder obtained from gels after drying and calcinating at 300°C, 600°C and 800°C with $10 \frac{^\circ\text{C}}{\text{min}}$ gradient and stayed in 2 hours, after then, they cooled in similar temperature gradient. Figures 2 and 3 show the amorphous structure for as-prepared and 300°C sample due to the short range ordering of the network [16]. Figures 4a and 4b, also show anatase and tenorite (CuO) phases. Anatase phase is tetragonal with crystalline system ($a=3.7850 \text{ \AA}$, $c=9.5140 \text{ \AA}$) and tenorite is monoclinic with crystalline system ($a=4.6530 \text{ \AA}$, $b=3.4100$, $c=5.1080 \text{ \AA}$).

Samples obtained from 600°C and 800°C have a high degree of the crystallinity and show anatase and tenorite phases. The grain size values were calculated from Scherrer equation:

$d = \frac{0.9\lambda}{2B \cos \theta}$, where $\lambda = 0.154 \text{ nm}$, and θ is the reflection angle.

As show in Figures 2 and 3, there is not rutile phase (no peak at $2\theta=27^\circ$), on the other hand, pure-anatase phase in TiO_2 polymorphs is available. Depending on crystalline size, distribution and arrangement, the anatase phase can transform into rutile phase at temperature between 400 and 1000 °C, but usually between 600 and 800°C in the nanocrystalline case [17]. Phase transformation depends on two main factors: surface energy and precursor chemistry. At nano size particles, the surface energy is a chief part of the total energy. It has been reported that the surface energy of the anatase phase is lower than those of rutile and brookite [18 and 19]. Precursor chemistry, experimental condition and presence of dopant material, influence on the nucleation and growth of the different polymorphs of TiO_2 [20-21]. Rutile crystals grow much faster than anatase [22], therefore, rutile nanocrystals exhibit larger diameters [23]. To retain nanocrystalline anatase phase on purpose that requires high temperature treatment that is important to prevent the anatase-to-rutile transition and restrict the growth of crystals when the material is heated. Zener pinning could be used to restrict the growth of nanocrystalline metal oxide in sol-gel method during the calcination stage [24-25]. This process involves the dopant material, such as silica, which exists as discrete particles at the nanocrystal interfaces and pins the grain boundaries in place by restricting surface diffusion and reducing the radius of curvature of nanoparticles [26]. In our knowledge, tenorite phase effects on elimination the rutile phase is so considerable, so that it has not been reported yet. The SiO_2 dopant can only limit the anatase-to-rutile transition and decreases the crystallization of rutile phase [27]. Since the atomic radii of Si atom is smaller than Ti, the TiO_2 particle experiences a contraction and its crystalline grows is retarded due to the Si atom. However, high composition of SiO_2 component leads to the formation of larger second particles of TiO_2 . This is due to the SiO_2 which behaves as a “neck” and connects the TiO_2 particles [26].

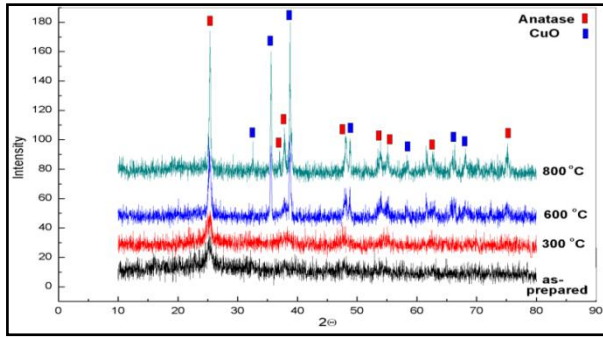


Fig. 2. XRD patterns of $\text{TiO}_2\text{-CuO-SiO}_2$ for molar ratio (MR=0.5) correspond to Table 1 obtained from: without hydrothermal treatment (as-prepared), calcined at 300 °C, calcined at 600 °C and calcined at 800 °C.

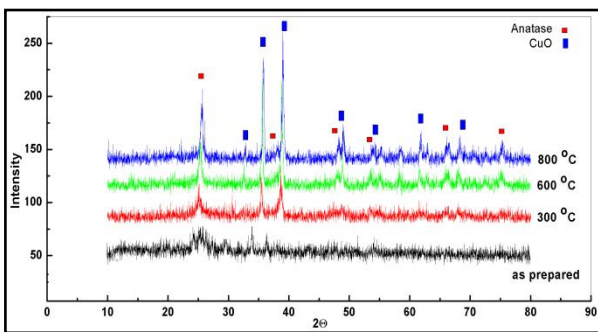


Fig. 3. XRD patterns of $\text{TiO}_2\text{-CuO-SiO}_2$ for molar ratio (MR=1) correspond to Table 1 obtained from: without hydrothermal treatment (as-prepared), calcined at 300 °C, calcined at 600 °C and calcined at 800 °C.

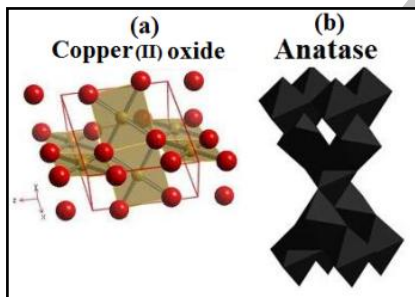


Fig. 4. Schematic model of (a) Tenorite and (b) anatase

Lattice strain of nanocrystallites are determined from the dependence of FWHM of diffraction lines observed in 2θ range of 10-80 on $\sin\theta$, according to the Williamson-Hall's equation: $\beta\cos\theta = \frac{k\lambda}{L} + 4\sin\theta$ [28], where β was FWHM observed, shape factor k was assumed to be 0.9 similar to Scherrer equation's. λ (wavelength of $K_\alpha(\text{Cu})$). The plots of $\beta\cos\theta$ against $4\sin\theta$ for different samples were approximated to be linear.

Lattice strain was determined from the slope of this linear relation. Because of lowly-crystallized powder samples, the linearity between $\beta\cos\theta$ and $4\sin\theta$ is not very evident [29]. The plots of $\beta\cos\theta$ against $4\sin\theta$ for different diffraction lines are illustrated in Figure 5 and Table 2. For low calcined temperatures, the experimental points for the diffraction lines measured scattered, because the peaks are weak and broad so that their FWHMs were difficult to be measured. As shown in Figure 6 for sample with specific molar ratio in precursor, variation of lattice strain per calcined temperature is illustrated. As can be seen in Figures 5 and 6 and Table 2 in, the lattice strain decreases with increasing the calcined temperature. For the samples with MR=0.5, with increasing the calcined temperature up to 300 °C, lattice strain decreases from -0.785 to -0.317 and with more increasing from 300 °C to 800 °C, lattice strain increases from 0.188 to 0.244. For the sample with MR=1, with increasing the calcined temperature, lattice strain decreases from 0.646 to 0.117. This implies that with increasing the calcined temperature, the form of lattice strain varies from internal to external strain.

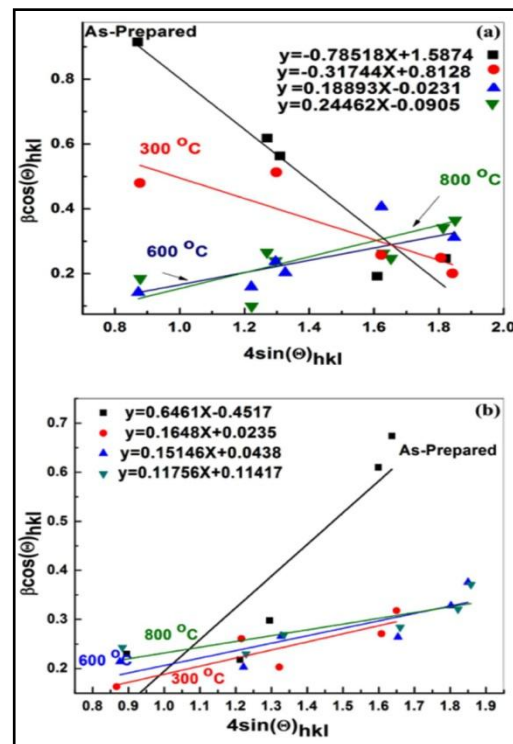


Fig.5. The relation between $\beta\cos\theta$ and $4\sin\theta$ (Williamson-Hall plots) for (a) MR=0.5 and (b) MR=1, with different calcination temperatures.

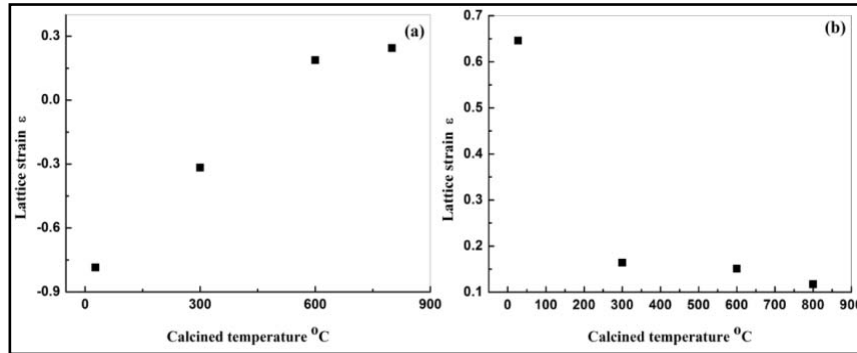


Fig. 6. Dependence of lattice strain on calcination temperature for (a) MR=0.5 and (b) MR=1.

Table 2. The 2 θ angle, d-space, Miller indexes, grain size of TiO₂-CuO-SiO₂.

Molar ratio TEOS/ TIOT / Cupper nitrate =1:1\0.5									
Sample	Anatase (Tetragonal)				CuO (Monoclinic)				Lattice Strain ϵ
	2 θ	d-spacing (Å)	Size (nm) (<i>h k l</i>)	Miller indices	2 θ	d-spacing (Å)	Size (nm) (<i>h k l</i>)	Miller indices	
As -prepared	25.36	3.50	8	(101)	There are no considerable peaks				-0.785
	37.9	2.37		(004)					
	48.01	1.89		(200)					
	53.80	1.70		(105)					
	54.91	1.67		(211)					
300 °C	25.36	3.50	15	(101)	38.43	2.32	17	(111)	-0.317
	38.10	2.34		(004)	35.54	2.51		($\bar{1}$ 11)	
	47.50	1.90		(200)	48.41	1.86		(202)	
	54.40	1.68		(105)	58.32	1.57		(202)	
	55.32	1.62		(211)	61.21	1.50		($\bar{1}$ 13)	
600 °C	25.15	3.51	23	(101)	38.69	2.32	46	(111)	0.188
	37.81	2.37		(004)	35.64	2.51		($\bar{1}$ 11)	
	48.14	1.89		(200)	48.71	1.86		($\bar{2}$ 02)	
	54.02	1.69		(105)	58.3	1.57		(202)	
	55.22	1.66		(211)	61.4	1.50		($\bar{1}$ 13)	
800 °C	25.30	3.50	45	(101)	38.79	2.31	101	(111)	0.244
	37.76	2.38		(004)	35.53	2.52		($\bar{1}$ 11)	
	48.04	1.88		(200)	48.87	1.86		(202)	
	53.93	1.70		(105)	58.32	1.58		(202)	
	55.12	1.66		(211)	61.58	1.5		($\bar{1}$ 13)	
Molar ratio TEOS/Cupper nitrate/TIOT=1:1\1									
As- prepared	25.46	3.49	14	(101)	There are no considerable peaks				0.646
	38.0	2.36		(004)					
	47.47	1.89		(200)					
	53.4	1.69		(105)					
	55.08	1.66		(211)					
300 °C	25.16	3.50	16	(101)	38.67	2.32	20	(111)	0.164
	38.10	2.36		(004)	35.35	2.53		($\bar{1}$ 11)	
	47.50	1.91		(200)	48.71	1.86		(202)	
	54.40	1.71		(105)	58.21	1.58		(202)	
	55.32	1.66		(211)	61.59	1.50		($\bar{1}$ 13)	
600 °C	25.38	3.50	18	(101)	38.84	2.31	30	(111)	0.151
	38.08	2.38		(004)	35.74	2.51		($\bar{1}$ 11)	
	47.97	1.89		(200)	48.86	1.86		($\bar{2}$ 02)	
	53.73	1.70		(105)	58.38	1.57		(202)	
	55.17	1.66		(211)	61.59	1.50		($\bar{1}$ 13)	
800 °C	25.55	3.48	22	(101)	39.06	2.30	45	(111)	0.117
	38.06	2.36		(004)	35.90	2.49		($\bar{1}$ 11)	
	48.01	1.88		(200)	49.02	1.86		(202)	
	53.95	1.69		(105)	58.3	1.58		(202)	
	55.12	1.66		(211)	61.81	1.49		($\bar{1}$ 13)	

The average crystal sizes of the nanopowders were calculated based on the Scherrer's formula. Figure 7 shows the variation of XRD crystal size (D) of nanoparticles prepared by the thermal treatment of nanopowders at different temperatures. It can be indicated that the crystal size of anatase in MR=0.5 increased rapidly from 23nm at 600 °C to 45nm at 800 °C and crystal size of anatase in MR=1 increased from 18nm at 600 °C to 22nm at 800 °C, while crystal size of CuO increased rapidly from 46nm to 101nm in MR=0.5. The size of grains decreases with increasing the molar ratio of precursors from 0.5 to 1 corresponds to Table 1. This is directly related to the crystallization of nanoparticles. Straight lines of

$\ln D$ against $1/T$ (Figure 8) are plotted according to the Scott [30] equation given below under the condition of homogeneous growth of nanocrystallites, which approximately describes the crystal growth during annealing: $D = C \exp(-E/RT)$ where C is a constant, E is the activation energy, R is the gas constant, and T is the absolute temperature. There exists a good linear relationship. The E value is calculated from the slope of the straight line as indicated in Table 3. It shows that the calcination temperature and molar ratio has a more remarkable effect on the growth of nanocrystallites. It can be indicated that by increasing the molar ratio, the activation energy is become smaller.

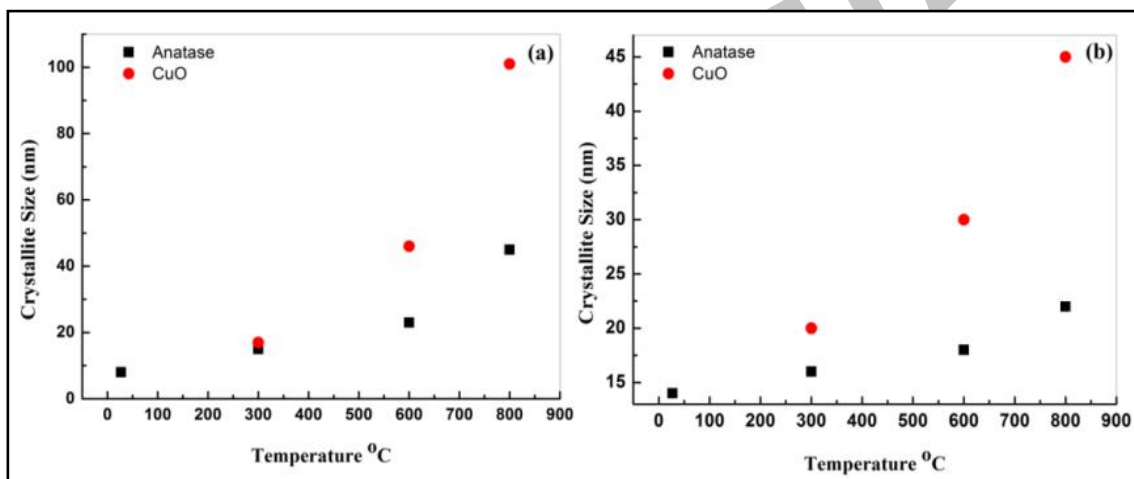


Fig. 7. Effect of thermal treatment temperature on crystallite size of anatase and CuO for (a) MR=0.5 and (b) MR=1.

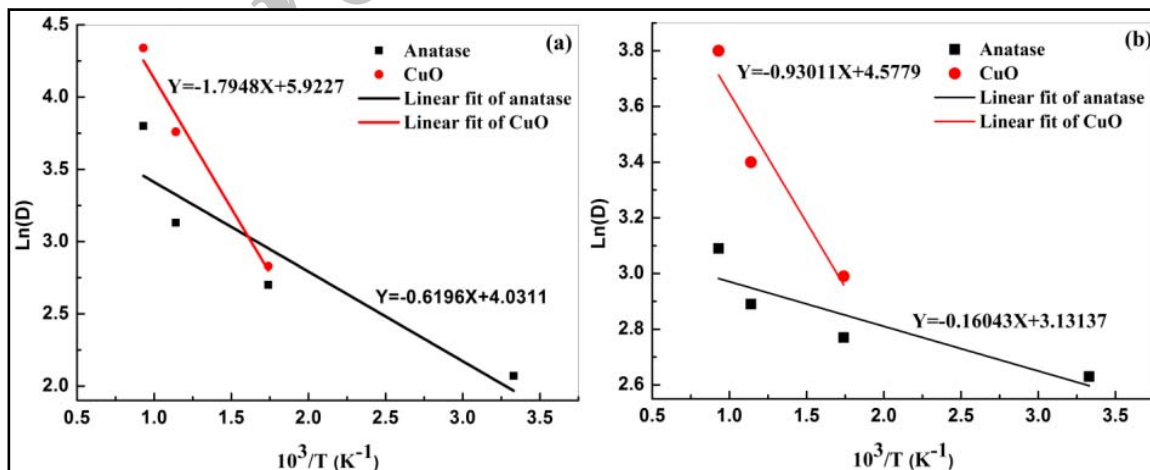


Fig. 8. Plot of $\ln D$ as a function of calcination temperature for (a) MR=0.5 and (b) MR=1.

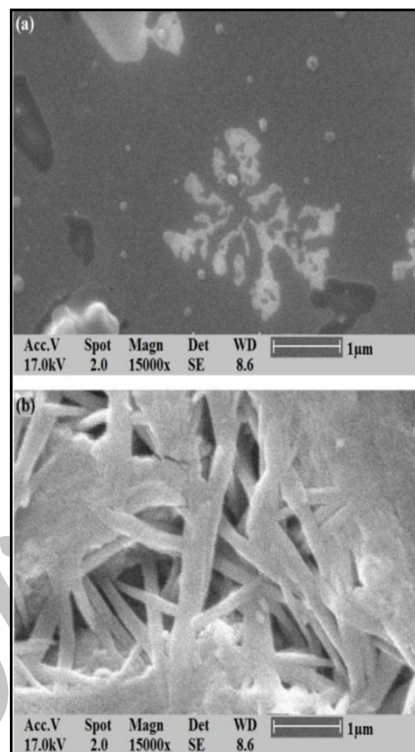
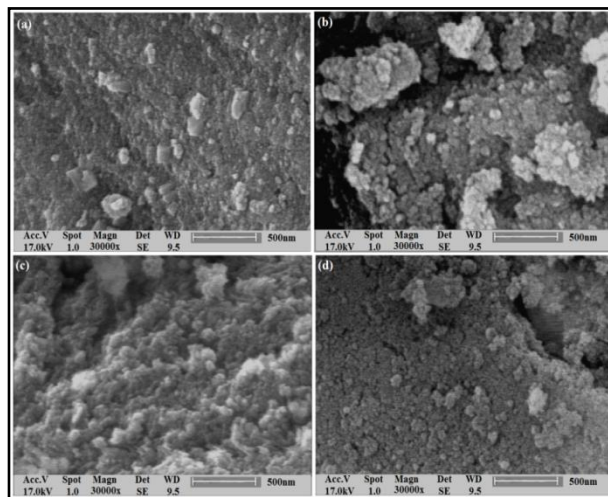
Table 3. Activation energy of formation crystalline phases for MR=0.5 and MR=1.

Molar ratio	0.5		1	
Crystallite phase	Anatase	CuO	Anatase	CuO
Activation energy kJ/mol	5.15	22.96	1.33	7.73

SEM images of $\text{TiO}_2\text{-CuO-SiO}_2$ nanopowders and coating are shown as Figures 9-11. In Figure 9 the coating on glass substrate at 300 °C but different molar ratio of precursors are shown. In Figure 9a with MR=0.5, that has a lower content of CuO, the surface smooth but in MR=1, the surface has fibers with arbitrary orientation. In Figure 10, as-prepared powder sample has regular surface and fine crystallinitis as observed in Figure 10a. By increasing the calcination temperature, particles are formed separately and spherical grains are represented. As shown in Figure 11, SEM images of powders with MR=1 but different calcined temperatures are presented. Nanoparticles have more congestion and density compared with MR=0.5 in Figure 10. In Figure 11a, the as-prepared state has rod structure and with increasing the calcined temperature, nanoparticles become separate spherical-shape. It is obvious that larger particle size is achieved by increasing the calcinations process and this is in good consistence with the Scherrer's equation in the XRD evaluation. In both molar ratio states, by increasing the calcinations temperature, the shape of particles become more granular and form separate particles.

The presence of the participants in two different molar ratios for powders and films according to Table 1 were confirmed by EDX spectra (Figures 12 and 13). As can be seen in Table 4, the results indicated the presence of TiO_2 , CuO and SiO_2 in the powder and film samples. Samples with MR=1 have more CuO content in composite than samples with MR=0.5. There are two separate morphology phases in as-prepared (MR=1) sample that is shown in Figure 14. In Figure 14, the rod region has more CuO content in composition than the region corresponding to

agglomerated particles and this issue is in good agreement with coating samples.

**Fig. 9.** SEM images of $\text{TiO}_2\text{-CuO-SiO}_2$ coating on glass calcined at 300 °C for (a) MR=0.5 and (b) MR=1.**Fig. 10.** SEM images of powder samples for MR=0.5 (a) as-prepared, (b) 300 °C, (c) 600 °C, (d) 800 °C.

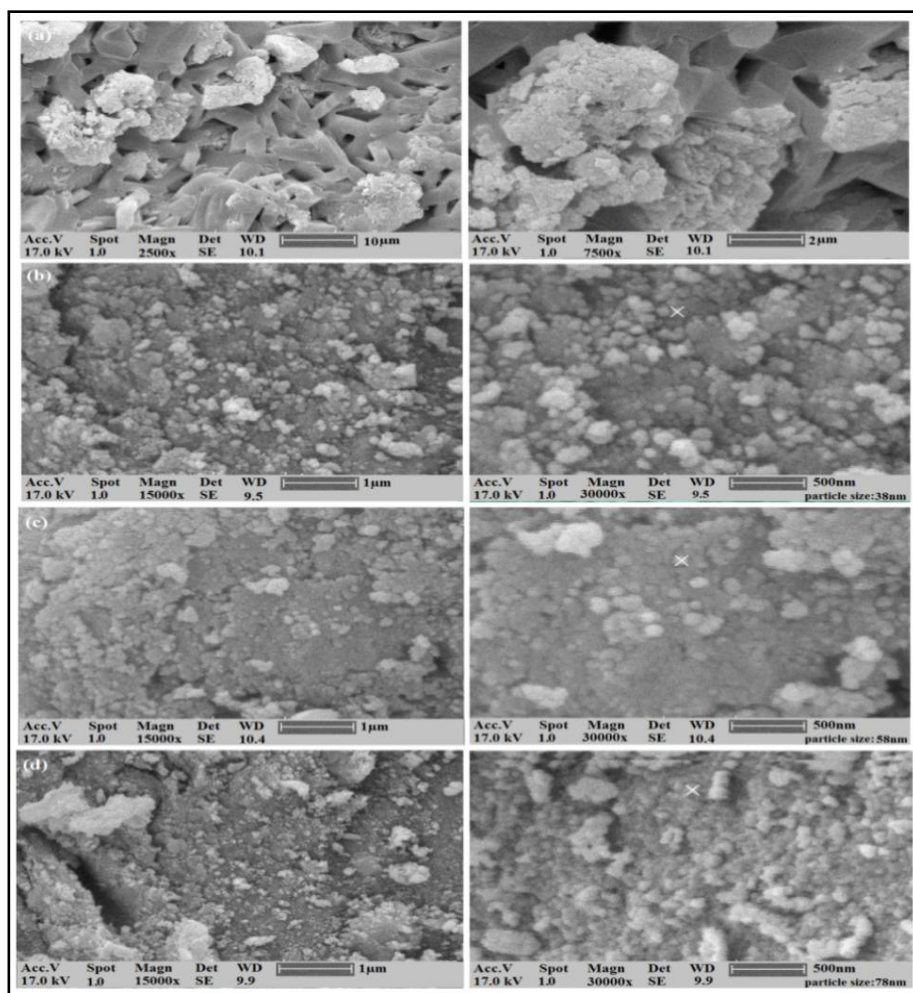


Fig. 11. SEM images of powder samples for MR=1 (a) as-prepared and calcined at: (b)300 °C, (c) 600 °C, (d) 800 °C.

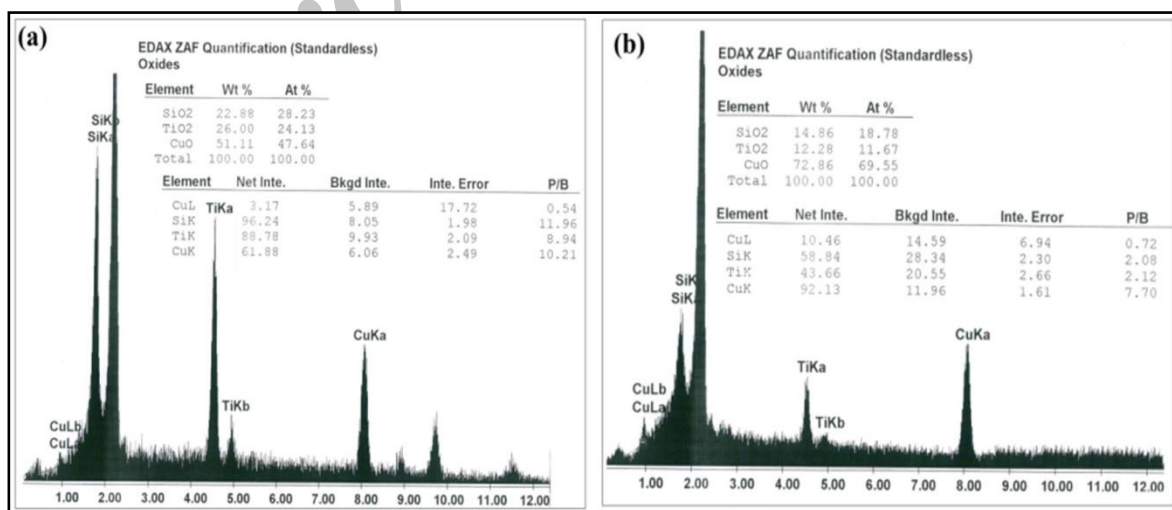


Fig. 12. EDX results for powder composite: (a) oxide analysis for MR=0.5 and (b) oxide analysis for MR=1.

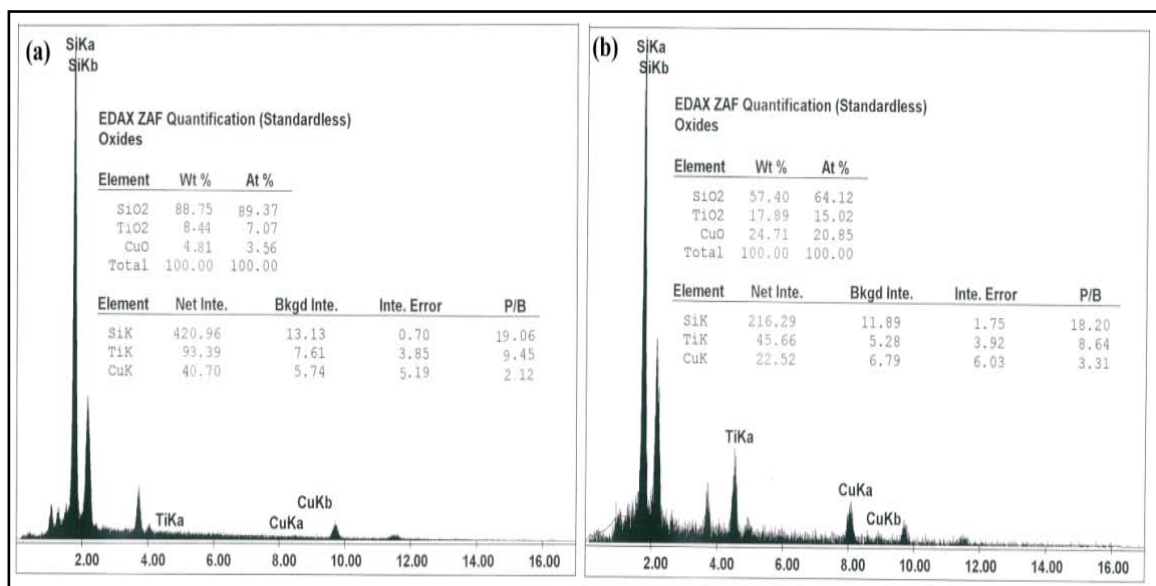


Fig. 13. EDX results for coating samples: (a) oxide analysis for MR=0.5 and (b) oxide analysis for MR=1.

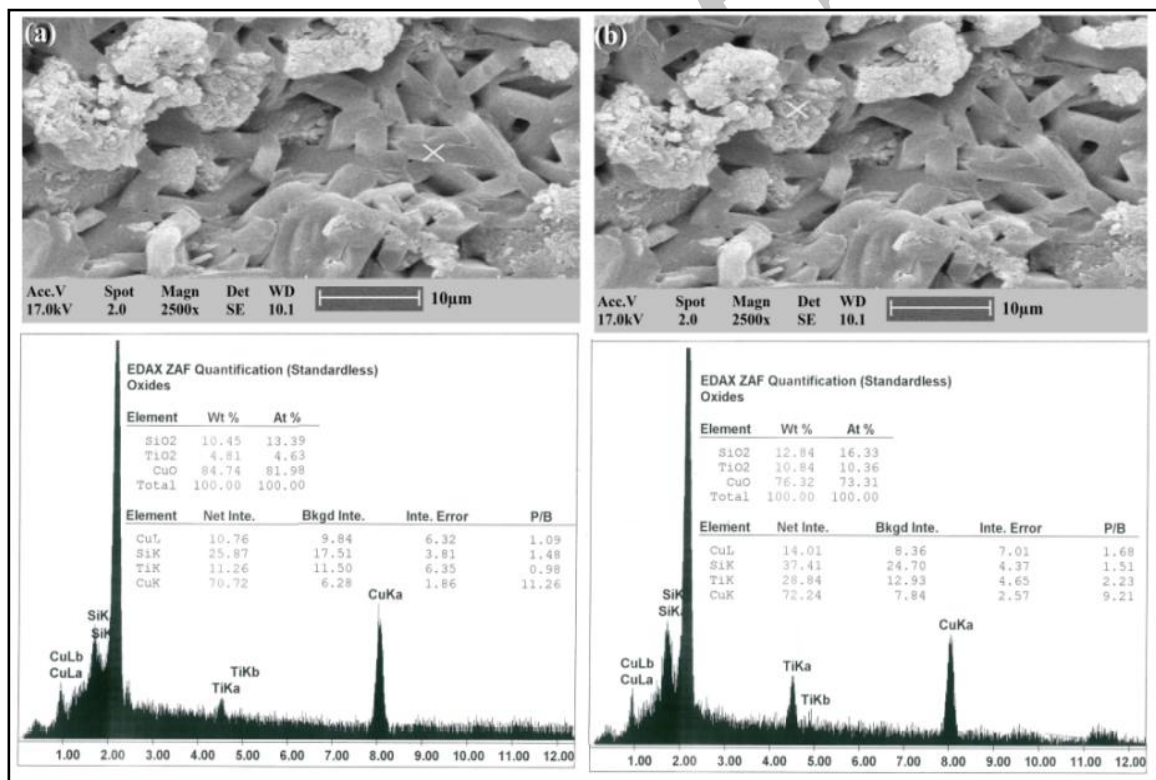


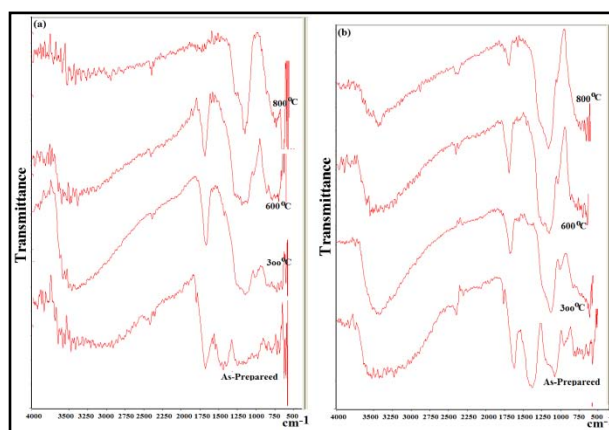
Fig. 14. EDX results for powder sample in as-prepared state MR=1: (a) rod region and (b) agglomerate region.

Table 4. Chemical composition obtained from EDX.

Powder sample MR=0.5			
Element	Weight percent	Atomic percent	Error(%)
SiO ₂	22.88	28.23	1.98
TiO ₂	26.00	24.13	2.09
CuO	51.11	47.64	2.49
Powder sample MR=1			
SiO ₂	14.86	18.78	2.30
TiO ₂	12.28	11.67	2.66
CuO	72.86	69.55	1.61
Coating sample MR=0.5			
SiO ₂	88.75	89.37	0.7
TiO ₂	8.44	7.07	3.58
CuO	4.81	3.56	5.19
Coating sample MR=1			
SiO ₂	57.40	64.12	1.75
TiO ₂	17.89	15.02	3.92
CuO	24.71	20.85	6.03

The FTIR spectra of different calcinations temperature of TiO₂-CuO-SiO₂ powder were recorded in the wave number range of 400-4000 cm⁻¹ (Figure 15). The polytitanosiloxane-tenorite composite of each sample shows the fundamental vibration modes. In the prepared gel, the 3200 cm⁻¹ band has to be attributed to hydroxyl groups (Ti-OH) and to OH from water and ethanol which are occluded in the titania pore. The OH bending band of water in the gel is observed at 1650 cm⁻¹ and the low energy interval the Ti-O band are found at 1061 and below 1000 cm⁻¹. The IR spectra show peaks characteristic of Ti-O-Ti (495–436 cm⁻¹). However the absorption peak at 1090 cm⁻¹ and 1010 cm⁻¹ indicates the Si-O-Si linkage in the powder form. The absorption peak of Si-O-Ti linkage was observed at 925 cm⁻¹. In dye-sensitized solar cells, functionalization of TiO₂ thin films with siloxane adsorbates has been shown to be useful as a surface passivation technique that hinders the recombination processes and improves the overall efficiency of light-to-electricity conversion [27]. When the composite was calcined at 800 °C, the high energy stretching band almost fades and the 1650 cm⁻¹ bending vibration band intensity decreases due to the vaporization of the

liquid. In the low energy interval, the band at 550 cm⁻¹ is due to stretching vibrations Cu-O and the broad bands between 800 and 1400 cm⁻¹ are attributed to the lattice vibrations of titanium oxide. It should be noted that no traces of solvents such as ethanol and water have been observed in calcined oxide composite. There are no difference between FTIR spectra of MR=0.5 and MR=1 samples.

**Fig. 15.** FTIR spectra of TiO₂-CuO-SiO₂ composite calcined at different temperature for (a) MR=0.5 and (b) MR=1.

CONCLUSION

Experimental results indicated that the homogeneous hydrolysis of tetra isopropyl ortho titanate via sol-gel route is a promising technique for preparing material with uniform nanoparticles. In this study, nanocrystalline $\text{TiO}_2\text{-CuO-SiO}_2$ particles have been successfully synthesised by chemical method and heat treatment process. The effect of $\text{TiO}_2\text{-CuO-SiO}_2$ composite on the structural properties of powders and films prepared by sol-gel (spin coating) technique has been examined. The XRD spectra showed anatase and CuO (Tenorite) phases and grains size. Average size of the grains ranged from 8 to 101 nm at 300 to 800 °C for MR=0.5 and 14 to 45nm for MR=1 respectively. The size of grains decreases with increasing the molar ratio of precursors from 0.5 to 1, correspond to Table 1. Scanning electron microscopy measurements showed nanostructure and morphology of powders and films. The as-prepared state has rod structure and by increasing the calcinations temperature, the shape of particles becomes more granular and forms separate particles. Chemical composition of samples was determined with EDX. The rod region has more CuO content in composition from the region corresponding to agglomerated particles and this issue is in good agreement with coating samples. To our knowledge, tenorite phase effects on elimination the rutile phase is so considerable that it has not been reported yet. It was shown that with increasing the calcined temperature, crystallite size increased, lattice strain decreased for MR=1 but for the samples with MR=0.5, with increasing the calcined temperature up to 300 °C, lattice strain decreased from -0.785 to -0.317 and with more increasing from 300 °C to 900 °C lattice strain increased from 0.188 to 0.244. It can be indicated that by increasing the molar ratio, the activation energy decreases. FTIR spectra of the ternary composite was presented and showed the possible bonds Si-O-Ti, Ti-O, Cu-O, Ti-O-Ti, Ti-OH and Si-O-Si.

REFERENCES

[1] Ennaoui A., Sankapal B. R., Skryshevsky V., lux-Stiener M. C., (2006), TiO_2 and $\text{TiO}_2\text{-SiO}_2$

- thin films and powders by one-step soft-solution method: Synthesis and characterizations. *Sol Energy Matter. Sol cellsm.* 90:1533-1541.
- [2] Zhang L., Yan S., Tian B., Zhang J., Anpo M., (2006), Preparation of $\text{TiO}_2\text{-SiO}_2$ film with high photocatalytic activity on PET substrate *Mat. Lett.* 60: 396-399.
- [3] Tsuji H., Sagimori T., Kurita K., Gotoh Y., Ishikawa J., (2002), Surface modification of TiO_2 (rutile) by metal negative ion implantation for improving catalytic properties. *Surf. Coat. Techn.*: 158-159: 208-213.
- [4] Kim S. J., Park S. D., Jeong Y. H., Park S., (1999), Homogeneous precipitation of TiO_2 ultrafine powders from aqueous TiOCl_2 solution, *Journal of the American Ceramic Society.* 82 : 927-932.
- [5] Ding Z., Hu X. J., Lu G. Q., Yue P. L., Greenfield P. F., (2000), Novel silica gelsupported TiO_2 photocatalyst synthesized by CVD method, *Langmuir.* 16: 6216-6222.
- [6] Yang J., Mei S., Ferreira J. M. F., (2001), Hydrothermal synthesis of nanosized titania powders: influence of tetraalkyl ammonium hydroxides on particle characteristics *Journal of the American Ceramic Society.* 8: 1696-1702.
- [7] Iwamoto S., Tanakulrungsank W., Inoue M., Kagawa K., Praserttham P., (2001), Synthesis of large-surface area silica-modified titania ultrafine particles by the glycothermal method. *J. of Mat. Sci. Lett.* 19 : 1439-1443.
- [8] Kato K., Tsuzuki A., Taoda H., Torii Y., Kato T., Butsugan Y., (1994), Crystal Structures of TiO_2 Thin Coatings Prepared from the Alkoxide Solution via the Dip-Coating Technique Affecting the Photocatalytic Decomposition of Aqueous Acetic Acid *J. Mater. Sci.* 29: 5911-15.
- [9] Abe Y., Sugimoto N., Nagao Y., T. Misono, (1988), Preparation of Monolithic $\text{SiO}_2\text{-TiO}_2$ Gels by Condensation Polymerization of Silicic Acid and Titanium Chelates. *J. Non-Cryst. Solids.* 104: 164-69.
- [10] Scott R., Maclachlan M., Ozin G., Curr O., (1999), Synthesis of Metal Sulfide Materials with Controlled Architecture. *Solid State Mater. Sci.* 4: 113-121.

- [11] Li M. M., Lebeau B., Mann S., (2003), Synthesis of aragonite nanofilament networks by mesoscale self-assembly and transformation in reverse microemulsions. *Adv. Mater.* 15: 2032–2035.
- [12] J. H. Lee, S.Y. Choi, C.E. Kim, (1997), The effects of initial sol parameters on the microstructure and optical transparency of TiO₂–SiO₂ binary aerogels. *J. Mater. Sci.* 32: 3577–3585.
- [13] Doeuff S., Henry M., Sanchez C., (1990), Sol-gel synthesis and characterization of titanium oxo-acetate polymers. *Mat. Res. Bull.* 25(12): 1519–1529.
- [14] Doeuff S., Henry M., Sanchez C., Livage J., (1987), Hydrolysis of the titanium alkoxides: modification of the molecular precursor by acetic acid. *J. Non-Crystall. Solids.* 89: 206–216.
- [15] Wolf C., Rüssel C., (1992), Sol-gel formation of zirconia: preparation, structure and rheology of sols. *J. Mater. Sci.* 27: 3749–3755.
- [16] Hochbaum A. I., Fan R., He R., Yang P., (2005), Controlled Growth of Si Nanowire Arrays for Device Integration. *Nano Lett.* 5: 457–460.
- [17] Barnard A. S., Zapol P., (2004), Effects of particle morphology and surface hydrogenation on the phase stability of TiO₂. *Phys. Rev. B*, 70: 235403–235416.
- [18] Navrotsky A., (2003), Energetics of nanoparticle oxides: interplay between surface energy and polymorphism. *Geochem. Trans.* 4: 34.
- [19] Naicker P. K., Cummings P. T., Zhang H., Banfield J. F., (2005), Characterization of Titanium Dioxide Nanoparticles Using Molecular Dynamics Simulations. *J. Phys. Chem. B* 109: 15243–15249.
- [20] Li J. G., Ishigaki T., Sun X., (2007), Anatase, Brookite, and Rutile Nanocrystals via Redox Reactions under Mild Hydrothermal Conditions: Phase Selective Synthesis and Physicochemical Properties. *J. Phys. Chem. C* 111(13): 4969–4976.
- [21] Yin H., Wada Y., Kitamura T., Kambe S., Murasawa S., Mori H., Sakata T., Yanagida S., (2001), Hydrothermal synthesis of nanosized anatase and rutile TiO₂ using amorphous phase. *TiO₂. J. Mater. Chem.* 11: 1694–1703.
- [22] Khlomanov I. N., Barborini E., Vinati S., Piseri P., Podesta A., Ducati C., Lenardi C., Milani P., (2003), The influence of the precursor clusters on the structural and morphological evolution of nanostructured TiO₂ under thermal annealing. *Nanotechnology*, 14:1168–1173.
- [23] Zhu K. R., Zhang M. S., Hong J. M., Yin Z., (2005), Size effect on phase transition sequence of TiO₂ nanocrystal. *Mater. Sci. Eng. A* 403: 87–93.
- [24] O'Dell L. A., Savin S. L. P., Chadwick A. V., Smith M. E., (2007), A ²⁷Al, ²⁹Si, ²⁵Mg and ¹⁷O NMR investigation of alumina and silica Zener pinned, sol-gel prepared nanocrystalline ZrO₂ and MgO. *Faraday Discuss.* 134: 83–102.
- [25] Chadwick A. V., Savin S. L. P., O'Dell L. A., Smith M. E., (2006), Keeping it small - restricting the growth of nanocrystals. *J. Phys.: Condens. Matter*, 18: 163–170.
- [26] O'Dell L. A., Savin S. L. P., Chadwick A. V., Smith M. E., (2007), Structural Characterization of SiO₂ and Al₂O₃ Zener-Pinned Nanocrystalline TiO₂ by NMR, XRD and Electron Microscopy. *J. Phys. Chem. C* 111: 13740–13746.
- [27] Riazian M., Bahari A., (2010), Structural Characterization of SiO₂ Zener-Pinned Nanocrystalline TiO₂ by XRD and SEM, *NanoThailand Conference*. 318–323.
- [28] Carp O., Huisman C.L., Reller A., (2004), Photoinduced reactivity of titanium dioxide. *Prog. Solid State Chem.* 32: 33–177.
- [29] Inagaki M., Nonaka R., Tryba B., Morawski A.W., (2006), Dependence of photocatalytic activity of anatase powders on their crystallinity. *Chemosphere*, 64: 437–445.
- [30] Scott M.G., (1983), Amorphous Metallic Alloys, *Butterworth, London*, p.151.

Cite this article as: M. Riazian *et al.*: Structure, effect of lattice strain and effect of sol concentration on the characterization of TiO₂-CuO-SiO₂ nanoparticles
Int. J. Nano Dimens. 3(2): 127-139, Autumn 2012

Archive of SID